

# Fabry–Pérot Cavity Sensors for Multipoint On-Column Micro Gas Chromatography Detection

Jing Liu,<sup>†,‡</sup> Yuze Sun,<sup>†,‡</sup> Daniel J. Howard,<sup>‡</sup> Greg Frye-Mason,<sup>§</sup> Aaron K. Thompson,<sup>||</sup> Shiou-jyh Ja,<sup>||</sup> Siao-Kwan Wang,<sup>⊥</sup> Mengjun Bai,<sup>⊥</sup> Haskell Taub,<sup>⊥</sup> Mahmoud Almasri,<sup>#</sup> and Xudong Fan<sup>\*,†,‡</sup>

Department of Biomedical Engineering, University of Michigan, 1101 Beal Avenue, Ann Arbor, Michigan 48109, Department of Biological Engineering, Bond Life Sciences Center, University of Missouri, Columbia, Missouri 65211, ICx Biodefense, 4343 Pan American Freeway NE, Suite 234, Albuquerque, New Mexico 87107, ICx Nomadics, 1024 South Innovation Way, Stillwater, Oklahoma 74074, Department of Physics and Astronomy, 223 Physics Building, and Department of Electrical and Computer Engineering, 233 Engineering Building West, University of Missouri, Columbia, Missouri 65211

We developed and characterized a Fabry–Pérot (FP) sensor module based micro gas chromatography ( $\mu$ GC) detector for multipoint on-column detection. The FP sensor was fabricated by depositing a thin layer of metal and a layer of gas-sensitive polymer consecutively on the endface of an optical fiber, which formed the FP cavity. Light partially reflected from the metal layer and the polymer–air interface generated an interference spectrum, which shifted as the polymer layer absorbed the gas analyte. The FP sensor module was then assembled by inserting the FP sensor into a hole drilled in the wall of a fused-silica capillary, which can be easily connected to the conventional gas chromatography (GC) column through a universal quick seal column connector, thus enabling on-column real-time detection. We characterized the FP sensor module based  $\mu$ GC detector. Sensitive detection of various gas analytes was achieved with subnanogram detection limits. The rapid separation capability of the FP sensor module assembled with both single- and tandem-column systems was demonstrated, in which gas analytes having a wide range of polarities and volatilities were well-resolved. The tandem-column system obtained increased sensitivity and selectivity by employing two FP sensor modules coated with different polymers, showing great system versatility.

The increasing demand for rapid on-site chemical vapor detection capability and low sample/power consumption in various fields such as environmental monitoring, homeland security, defense, and biomedicine requires portable micro gas chromatography ( $\mu$ GC) analyzers.<sup>1–7</sup> During several decades of research

and development,  $\mu$ GC has undergone significant breakthroughs, especially with respect to miniaturization and rapid detection. Current  $\mu$ GC systems often use a short capillary column<sup>8,9</sup> or a microfabricated rectangular column<sup>3–6,10–15</sup> with attached heating components to satisfy the requirements on system size and detection speed. However, these improvements are usually obtained at the cost of the most essential separation capability for gas chromatography (GC), owing to insufficient interaction of the short  $\mu$ GC columns with analytes.

To improve the separation capability and selectivity of  $\mu$ GC analyzers, researchers have developed a tandem-column system with each column being coated with a different polymer,<sup>8,16–22</sup> which is intended to separate a wide range of samples more efficiently, thus compensating for the deficiency of short length. Unfortunately, the tandem-column based  $\mu$ GC still inevitably suffers from the same coelution problem as in a short single-column  $\mu$ GC, i.e., analytes already separated from the first column

- (4) Kolesar, E. S., Jr.; Reston, R. R. *IEEE Trans. Compon., Packag., Manuf. Technol.* **1998**, *21*, 324–328.
- (5) Overton, E. B.; Carney, K. R.; Roques, N.; Dharmasena, H. P. *Field Anal. Chem. Technol.* **2001**, *5*, 97–105.
- (6) Noh, H.-S.; Hesketh, P. J.; Frye-Mason, G. C. *J. Microelectromech. Syst.* **2002**, *11*, 718–725.
- (7) Cai, Q. Y.; Zellers, E. T. *Anal. Chem.* **2002**, *74*, 3533–3539.
- (8) Lu, C.-J.; Whiting, J.; Sacks, R. D.; Zellers, E. T. *Anal. Chem.* **2003**, *75*, 1400–1409.
- (9) Staples, E. J.; Viswanathan, S. *IEEE Sens. J.* **2005**, *5*, 622–631.
- (10) Lambertus, G.; Elstro, A.; Sensening, K.; Potkay, J.; Agah, M.; Scheuring, S.; Wise, K.; Dorman, F.; Sacks, R. *Anal. Chem.* **2004**, *76*, 2629–2637.
- (11) Lorenzelli, L.; Benvenuto, A.; Adami, A.; Guarnieri, V.; Margesin, B.; Mulloni, V.; Vincenzi, D. *Biosens. Bioelectron.* **2005**, *20*, 1968–1976.
- (12) Lambertus, G.; Sacks, R. *Anal. Chem.* **2005**, *77*, 2078–2084.
- (13) Stadermann, M.; McBrady, A. D.; Dick, B.; Reid, V. R.; Noy, A.; Synovec, R. E.; Bakajin, O. *Anal. Chem.* **2006**, *78*, 5639–5644.
- (14) Reidy, S.; Lambertus, G.; Geece, J.; Sacks, R. *Anal. Chem.* **2006**, *78*, 2623–2630.
- (15) Reidy, S.; George, D.; Agah, M.; Sacks, R. *Anal. Chem.* **2007**, *79*, 2911–2917.
- (16) Rowe, M. P.; Steinecker, W. H.; Zellers, E. T. *J. Environ. Monit.* **2007**, *8*, 270–278.
- (17) Jones, J. R.; Purnell, J. H. *Anal. Chem.* **2002**, *62*, 2300–2306.
- (18) Deans, D. R.; Scott, I. *Anal. Chem.* **2002**, *45*, 1137–1141.
- (19) Purnell, J. H.; Wattan, M. H. *Anal. Chem.* **2002**, *63*, 1261–1264.
- (20) Veriotti, T.; Sacks, R. *Anal. Chem.* **2001**, *73*, 813–819.
- (21) Libardon, M.; McGuigan, M.; Yoo, Y. J.; Sacks, R. *J. Chromatogr., A* **2005**, *1086*, 151–159.
- (22) Sacks, R.; Coutant, C.; Veriotti, T.; Grail, A. *J. Sep. Sci.* **2000**, *23*, 225–234.

\* To whom correspondence should be addressed. E-mail: xsfan@umich.edu.

<sup>†</sup> Department of Biomedical Engineering, University of Michigan.

<sup>‡</sup> Department of Biological Engineering, University of Missouri.

<sup>§</sup> ICx Biodefense.

<sup>||</sup> ICx Nomadics.

<sup>⊥</sup> Department of Physics and Astronomy, University of Missouri.

<sup>#</sup> Department of Electrical and Computer Engineering, University of Missouri.

(1) Terry, S. C.; Jerman, J. H.; Angell, J. B. *IEEE Trans. Electron Devices* **1979**, *26*, 1880–1886.

(2) Angell, J. B.; Terry, S. C.; Barth, P. W. *Sci. Am.* **1983**, *248*, 44–45.

(3) Yu, C. M.; Lucas, M.; Koo, C.; Stratton, P.; DeLima, T.; Behymer, E. *Am. Soc. Mech. Eng., Dyn. Syst. Control Div. (Publ.)* **1998**, *66*, 481–486.

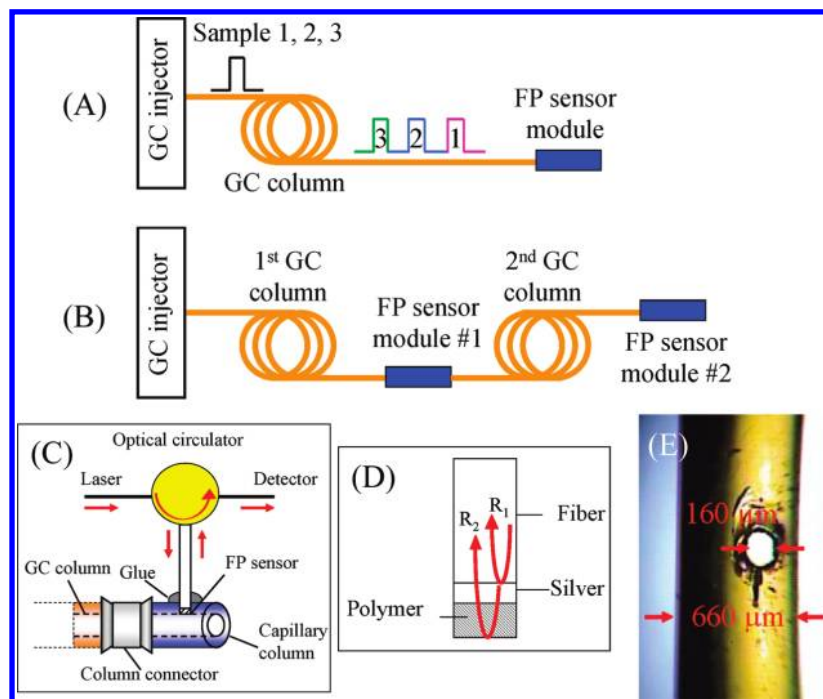


**Figure 1.** (A) Schematic of the single-column system. The FP sensor module was connected to the GC injection port through a 1.6 m long GC guard column, followed by a 1.3 m long Carbowax GC column. (B) Schematic of the tandem-column system. The first FP sensor module was connected to the end of the first 0.9 m long RTX-1 GC column, and the second FP sensor module was connected to the end of the second 0.2 m long Carbowax GC column. (C) Detailed structure of the FP sensor module assembled by inserting an FP sensor probe into a hole drilled in a fused-silica capillary. An optical circulator was used to deliver the laser light to the FP sensor and subsequently to the detector. (D) Schematic of the FP sensor probe fabricated by sequentially coating the endface of a single-mode optical fiber with silver and polymer. The two optical beams ( $R_1$  and  $R_2$ ) reflected by the silver and polymer layer form the interference pattern shown in Figure 2. (E) Picture of the hole drilled in a fused-silica capillary. Dimensions in panels A–D are not to scale.

may coelute after passing through the second one.<sup>23</sup> Since traditional GC detectors carry out detections only at the terminal end of the tandem-column system, it is difficult to differentiate the coeluted analytes from each other. Current methods to solve this problem use a pressure valve<sup>8,20</sup> or a temperature control module<sup>21</sup> to modulate the retention times of the analytes. However, these methods may require samples to be tested several times under different conditions before they can be fully separated,<sup>24,25</sup> which significantly increases the operation complexity and the detection time.

In contrast, on-column detection provides a very promising approach to addressing the coelution problem. In this scheme, analytes are detected when they travel along the column, rather than after they elute out from the terminal end of the tandem-column system. The on-column detection scheme has the highly desirable feature of flexibility in selecting the detection location along the column.<sup>23</sup> Moreover, multiple detectors can be installed at predetermined locations along the column to independently measure the retention time of each analyte and provide complementary chromatograms. As a result, each analyte can be separated on at least one detection location in a single test without having to use any additional components, considerably simplifying the detection operation and system design.<sup>23</sup> Additionally, on-column detectors do not retain any analytes. Therefore, they do

not add any additional dead volumes, thus minimizing related peak broadening. Finally, since the gas flow is uninterrupted in the on-column detection scheme, analytes can easily be passed along to subsequent columns or instruments for further analysis. This feature offers a great potential to improve the detection selectivity and sensitivity by employing different detectors in a single  $\mu$ GC system.

Recently, an on-column detection scheme has been explored in the form of an optofluidic ring resonator (OFRR).<sup>23,26–29</sup> The OFRR was connected to a regular GC column and acted as both separation column and on-column detector. Rapid separation and detection capability have been obtained with the OFRR-based tandem-column system.<sup>23</sup> However, due to its thin-walled structure the OFRR is relatively fragile, making it difficult to implement in many field applications. In addition, since the OFRR column is coated with a single type of polymer for both separation and sensing purposes, it may be sensitive to only a certain class of analytes, which may limit its versatility in detecting a wide range of analytes.<sup>23</sup>

In this paper, we developed an alternative, highly versatile on-column detector for  $\mu$ GC systems (see Figure 1, parts A and B) based on a Fabry–Pérot (FP) cavity sensor module (see Figure

(23) Sun, Y.; Liu, J.; Howard, D. J.; Frye-Mason, G.; Thompson, A. K.; Ja, S.-j.; Fan, X. *Analyst* **2010**, *135*, 165–171.

(24) Whiting, J.; Sacks, R. *Anal. Chem.* **2001**, *74*, 246–252.

(25) Akard, M.; Sacks, R. *Anal. Chem.* **2002**, *66*, 3036–3041.

(26) Shopova, S. I.; White, I. M.; Sun, Y.; Zhu, H.; Fan, X.; Frye-Mason, G.; Thompson, A.; Ja, S.-j. *Anal. Chem.* **2008**, *80*, 2232–2238.

(27) Sun, Y.; Fan, X. *Opt. Express* **2008**, *16*, 10254–10268.

(28) Sun, Y.; Shopova, S. I.; Frye-Mason, G.; Fan, X. *Opt. Lett.* **2008**, *33*, 788–790.

(29) Sun, Y.; Liu, J.; Frye-Mason, G.; Ja, S.-j.; Thompson, A. K.; Fan, X. *Analyst* **2009**, *134*, 1386–1391.

1C). The FP sensor was fabricated by depositing a thin layer of metal and a layer of polymer sequentially on the endface of a single-mode optical fiber to form an FP cavity (see Figure 1D).<sup>30</sup> It was then inserted into a hole drilled in the wall of a fused-silica capillary. Light partially reflected from the metal and from the polymer–air interface creates an interference modulation. When an analyte travels along the sensor module, the polymer–analyte interaction changes the refractive index or the thickness of the polymer coated on the FP sensor, resulting in a spectral shift of the interference modulation, which can be detected quantitatively in real time.

The proposed FP sensor has a few distinctive advantages. First, the FP sensor is robust and easy to fabricate and handle, which makes it very attractive for mass production and field applications. Second, different sensing polymer layers can be coated on the FP sensors to accommodate the detection of a wide range of analytes. Third, since the FP sensor module can be easily connected to a GC column through a universal quick seal column connector, various types of GC columns with different lengths can be used in the tandem-column system to achieve great versatility in analyte detection.

Previously, we showed that the FP sensor is highly sensitive to volatile organic compounds (VOCs).<sup>30</sup> In this work, we further investigated the FP sensor as an on-column detector by assembling it with both single- and tandem-column systems (see Figure 1, parts A and B). We began by characterizing the FP-based on-column detector and then demonstrated the powerful separation capability of the FP-based  $\mu$ GC systems.

## EXPERIMENTAL SECTION

**Materials.** All the analytes used in the experiment were purchased from Sigma (St. Louis, MO) and had purity greater than 97%. RTX-1 (part no. 10105, inner diameter (i.d.) = 250  $\mu$ m) and guard columns (part no. 22335, i.d. = 250  $\mu$ m) were purchased from Restek (Bellefonte, PA). Carbowax-coated GC columns (part no. 24079, i.d. = 250  $\mu$ m) was purchased from Sigma. Fused-silica capillaries (outer diameter (o.d.) = 660  $\mu$ m, i.d. = 535  $\mu$ m) were purchased from Polymicro (Phoenix, AZ). Universal quick seal column connectors were purchased from Varian (Palo Alto, CA). Tin chloride, palladium chloride, hydrochloric acid, silver nitrate, hydrazine hydrate, ammonium carbonate, and ammonium hydroxide were purchased from Sigma. Poly(ethylene glycol) 1000 (PEG 1000) and poly(dimethylsiloxane) (PDMS) were purchased from Fluka (St. Louis, MO). Single-mode fibers (SMF-28) were purchased from Corning (Corning, NY). UV-curable optical glue was purchased from Dymax (Torrington, CT). All materials were used as received.

**FP Sensor Fabrication.** The details of the FP sensor fabrication were described in our previous report.<sup>30</sup> Briefly, it was fabricated by coating a thin layer of silver on the endface of a single-mode optical fiber (SMF-28), followed by depositing a polymer layer. The silver layer was coated by the electroless plating method.<sup>31</sup> A cleaved fiber was sensitized and catalyzed by immersing it in each of the following two solutions for 3 min. The sensitization solution was a mixture of tin chloride (10 g/L) and hydrochloric acid (40 mL/L) in DI water, whereas the catalyst

solution was a mixture of palladium chloride (0.5 g/L) and hydrochloric acid (40 mL/L) in DI water. Then, the fiber was immersed for about 2 min in the plating bath, which contained silver nitrate (0.002 g), ammonia in water (20%) (50  $\mu$ L), hydrazine hydrate (1  $\mu$ L), ammonium carbonate (0.02 g), and 1.6 mL of DI water. The thickness of the silver layer coated in this manner was on the order of tens of nanometers, which allowed about 10–20% of the light intensity to be reflected. The polymer layer was deposited by dip-coating, where the silver-coated fiber was immersed in the polymer solution and dried at room temperature. In the present work, we used PEG 1000 and PDMS as the polar and nonpolar coating layer, respectively, both having a thickness on the order of 2  $\mu$ m, as characterized by an atomic force microscope (AFM). The thickness of the PEG 1000 coating could be controlled by the polymer concentration in a solution of methanol, which will be discussed in detail in the characterization section. The FP sensor module was assembled by inserting the FP sensor into a hole (approximately 160  $\mu$ m in diameter, see Figure 1E) drilled near the center part of a short (approximately 5 cm) fused-silica capillary from Polymicro by a mechanical drilling machine (Sherline model 2000). The whole assembling process took place under a microscope to ensure that the end of the FP sensor was flush with the capillary inner wall to avoid any potential disturbance to the gas flow. Finally, the hole was sealed with a UV-curable optical glue.

**Experimental Setup.** The experimental setup is illustrated in Figure 1, parts A and B. For the single-column system (Figure 1A), the FP sensor module was connected to the GC injection port through a 1.6 m long GC guard column, followed by a 1.3 m long Carbowax-coated GC column. For the tandem-column system (Figure 1B), the first FP sensor module was installed at the end of the first 0.9 m long RTX-1 GC column, and the second one was at the end of the second 0.2 m long Carbowax GC column. Gas analyte extracted from the head space of the bottle containing the analyte by a solid-phase microextraction (SPME) fiber (PDMS/DVB, 65  $\mu$ m diameter fiber, Supelco 57310-U) was injected through the GC injector (HP 5890, heated to 250  $^{\circ}$ C). The linear installed had an i.d. of 0.75 mm. Ultrahigh purity (UHP) helium was used as carrier gas. The flow rate was 0.3 mL/min. GC columns and FP sensor modules were all kept at room temperature. For comparison purposes, we also used a flame ionization detector (FID) to detect the analyte. The FID temperature was set at 325  $^{\circ}$ C.

**FP Sensor Operation Principles.** Figure 1D shows the details of the FP sensor. Two beams of light reflected from the silver coating layer and from the polymer–air interface formed the interference signal, which is governed by

$$I = R_1 + R_2 + 2\sqrt{R_1R_2} \cos(\phi) \quad (1)$$

where  $R_1$  and  $R_2$  are the light intensity reflected from the silver layer and the polymer–air interface, respectively.

$$\phi = 4\pi nt/\lambda \quad (2)$$

where  $\lambda$  is the laser wavelength and  $n$  and  $t$  are the polymer refractive index and thickness, respectively. An example of the interference modulation is presented in Figure 2. The interaction between the polymer and the analyte results in a change in the

(30) Liu, J.; Sun, Y.; Fan, X. *Opt. Express* **2009**, *17*, 2731–2738.

(31) Cheng, Y. S.; Yeung, K. L. *J. Membr. Sci.* **1999**, *158*, 127–141.

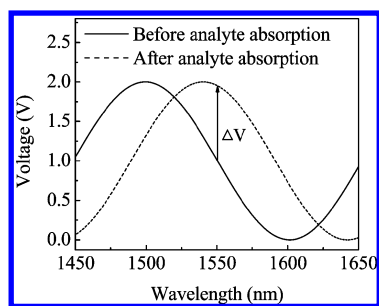


**Figure 2.** Example of the interference spectrum generated by the FP sensor probe based on eqs 1 and 2, where  $n = 1.47$  and  $t = 4 \mu\text{m}$ . The signal increases for the fixed laser wavelength centered around 1550 nm, when the interference spectrum shifts to a longer wavelength in response to the polymer–analyte interaction.

polymer thickness and/or refractive index and hence in the signal from the photodetector:

$$\Delta I = -2\sqrt{R_1 R_2} \sin(\phi) \Delta\phi \quad (3)$$

$\Delta I$  becomes the largest when  $\phi$  is chosen to be at the quadrature point, i.e.:

$$\phi = m2\pi + 3\pi/2 \quad (4)$$

where  $m$  is an integer, in which case

$$\Delta I/I \propto \Delta\phi \quad (5)$$

assuming  $R_1 = R_2$  for simplicity.

In our experiment, a 1550 nm tunable diode laser (JDS Uniphase, CQF935/28 28) was coupled into the FP sensor through an optical circulator (Thorlabs, 6015-3). The laser wavelength was tuned and fixed near the quadrature point around 1550 nm. The reflected light was detected by a photodetector (New Focus, 2033) located at the output port of the circulator. As exemplified in Figure 2, the signal changes in response to the polymer–analyte interaction. A home-built LABVIEW program was used to monitor the signal change in real time, and the data was recorded at a rate of 20 Hz.

## RESULTS AND DISCUSSION

**Characterization.** The potential of the FP sensor for rapid, on-column detection is demonstrated in Figure 3, where we show the sensor response to toluene, decane, methanol, and dimethyl methylphosphonate (DMMP), which have various volatilities and polarities. The voltage change resulting from the interaction between the analyte and the polymer layer depends on the amount of the analyte absorbed by the polymer coating layer. Since the FP sensor was coated with polar PEG 1000, different responses for polar and nonpolar analytes were expected.<sup>28</sup> For nonpolar and slightly polar analytes, such as toluene, decane, and methanol, which interact weakly with the polar polymer, a sharp peak was observed with a peak width of several seconds, as shown in Figure 3A–C. In contrast, the signal from highly polar DMMP, which interacts strongly with the polymer layer, returned slowly back to the baseline, as shown in Figure 3D.

In order to investigate further the temporal response of the FP sensor, we compare the FP results with those obtained from the FID using the same GC columns and flow rate. As shown in

Figure 3, the peak widths for nonpolar and slightly polar analytes (i.e., toluene, decane, and methanol) were comparable for the FP sensor and for the FID. The slightly increased retention time in the FID ( $\sim 10$  s) was due to the extra GC column used to link the  $\mu\text{GC}$  system to the FID. However, the peak of highly polar DMMP obtained from the FP sensor was much broader than the one obtained from the FID. This phenomenon can be attributed to the inherently different detection principles of the two sensors. The FID detects the ion current generated by burning analytes. As a result, its temporal response does not vary much for analytes with different polarities. In contrast, the FP sensor detects the interaction between the analyte and the polymer layer. Consequently, its temporal response reflects the polymer change in response to the absorption and desorption processes of analytes. While for nonpolar or slightly polar analytes, the absorption and desorption are very fast for PEG 1000, leading to at most a very small increase in the peak width, strong interaction between PEG 1000 and DMMP results in an additional broadening of the peak that has already been broadened by the 1.3 m long Carbowax-coated GC column.

In addition to the polymer polarity, polymer thickness may contribute to the peak broadening, as it takes time for analytes to diffuse into and out of the coating. Usually, for the analytes (such as toluene, decane, and methanol in Figure 3A–C) that have less interaction with the polymer coating (i.e., lower partition coefficients), a thicker polymer will not introduce significant peak broadening.<sup>29</sup> However, for DMMP, which has strong interaction with PEG 1000, the polymer thickness has a significant impact on the peak width, as shown in Figure 4.

Furthermore, we investigated the FP sensor response to various analyte masses. We selected two representative analytes, nonpolar decane and highly polar DMMP. Figure 5 plots the peak height as a function of analyte mass. A linear response was observed for both analytes, though DMMP started to saturate at the mass level larger than 20 ng. The sensitivity of the FP sensor for decane and DMMP was 4.75 and 77 mV/ng, respectively. This huge difference in sensitivity was caused by the different interactions between the analytes and the polymer coated on the FP sensor.

One major contribution to the noise in the FP sensor signal is from thermal fluctuations, as they induce the thickness change (thermal expansion effect) and the refractive index change (thermo-optic effect). The temperature-induced FP sensor signal change can be described by the following equation, based on eqs 2, 4, and 5:

$$\Delta I/I \propto \Delta\phi = \frac{4\pi}{\lambda} \Delta(nt) = (m2\pi + 3\pi/2) \left( \frac{\partial n}{\partial T} \frac{1}{n} + \frac{\partial t}{\partial T} \frac{1}{t} \right) \Delta T \quad (6)$$

where  $\Delta T$  is the temperature variation. For most polymers, the thermal expansion coefficient,  $\partial t/(t\partial T)$ , is usually around  $10^{-4} \text{ } ^\circ\text{C}^{-1}$ ,<sup>32,33</sup> and the thermo-optic coefficient,  $\partial n/\partial T$ , is around  $-10^{-4} \text{ } ^\circ\text{C}^{-1}$ .<sup>34</sup>  $m$  is usually on the order of 1 for the polymer thickness of  $1 \mu\text{m}$ ,  $\lambda = 1550 \text{ nm}$ , and  $n$  is approximately 1.5. Conse-

(32) Paul, R. S. *J. Polym. Sci.* **1962**, *56*, 403–407.

(33) Holliday, L.; Robinson, J. *J. Mater. Sci.* **1973**, *8*, 301–311.

(34) Zhang, Z.; Zhao, P.; Lin, P.; Sun, F. *Polymer* **2006**, *47*, 4893–4896.

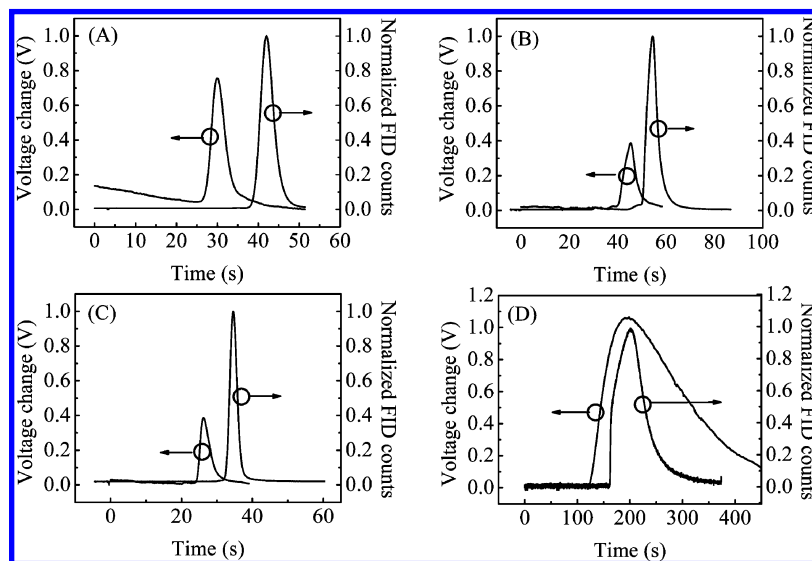


**Figure 3.** Response of the PEG 1000 coated FP sensor and the FID to (A) toluene, (B) decane, (C) methanol, and (D) DMMP. Peak heights from the FID were normalized to unity. The retention times of toluene, decane, methanol and DMMP from the FP sensor (FID) were 30.0 (42.0), 49.8 (58.8), 30.7 (39.1), and 192.3 s (200.3 s), respectively. The corresponding peak widths at half-maximum were 3.6 (3.5), 5.8 (5.0), 3.2 (2.4), and 164.0 s (66.7 s), respectively.

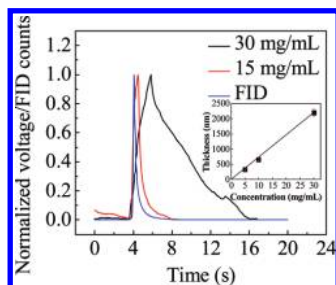


**Figure 4.** Comparison of the DMMP sensing response obtained from the FID and the FP sensors. The two FP sensors were dip-coated in the PEG 1000 in methanol solution with a concentration of 15 and 30 mg/mL, respectively. For the purpose of comparison, the FP sensor and the FID were connected directly to the GC injection port through a 1.6 m long GC guard column. The chromatograms obtained from the FP sensors are shifted so that they have the same response onset at the same time as that from the FID. The inset plots the relationship between the polymer layer thickness and the coating solution concentration. Three silicon wafers were used to simulate the coating event taking place on the FP sensor probe. They were dip-coated in the coating solution with the concentration of 30, 10, and 5 mg/mL, respectively. AFM was used to measure the polymer layer thickness on the silicon wafer. The corresponding thicknesses were 2.2  $\mu\text{m}$ , 660 nm, and 330 nm, respectively.

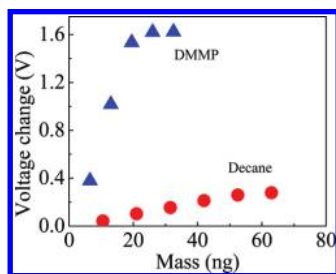


**Figure 5.** PEG 1000 coated FP sensor responses to decane and DMMP with various injected masses.

quently, the corresponding fractional intensity change should be on the order of  $10^{-3}$ – $10^{-4}$   $^{\circ}\text{C}^{-1}$ .

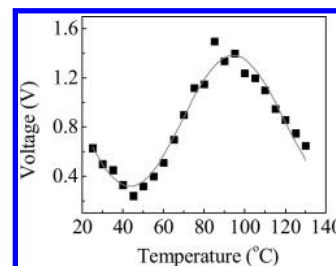


**Figure 6.** Temperature-dependent response of the PEG 1000 coated FP sensor. The solid line is the sinusoidal curve fit.

On the basis of the above discussion, we experimentally characterized the temperature response of the PEG 1000 coated FP sensor by placing it in a temperature-controlled oven. As expected, the signal change caused by the interference shift was sinusoidal as plotted in Figure 6. The highest temperature change was at the quadrature point with the estimated slope of 0.036  $\text{V}/^{\circ}\text{C}$ . Usually, the temperature stability of 0.01  $^{\circ}\text{C}$  can be achieved,<sup>26</sup> leading to a thermally related noise level on the order of 0.36 mV (which was  $4.2 \times 10^{-4}$  of the baseline signal 0.84 V at 23 or 70  $^{\circ}\text{C}$ ) and hence a detection limit of approximately 75 and 5  $\mu\text{g}$  for decane and DMMP, respectively. However, it should be noted that, in addition to thermally induced noise, electronic noise and laser source noise may contribute to the total system noise. Currently, our system has a noise level of 7 mV, which results in a detection limit of approximately 50  $\mu\text{g}$  for DMMP (see Figure S1 in the Supporting Information). Future improvement in data acquisition and in optical design will certainly lower the noise in these aspects.

**Demonstration of On-Column GC Detectors.** The separation/detection capability of the FP sensor module assembled with both single- and tandem-column systems is demonstrated in Figure 7. In the single-column system (Figure 1A), a mixture of four different analytes was injected through the GC injection port, which was separated as it traveled through the 1.6 m long GC guard column, followed by a 1.3 m long Carbowax-coated GC column. The separated analytes were detected by the FP sensor

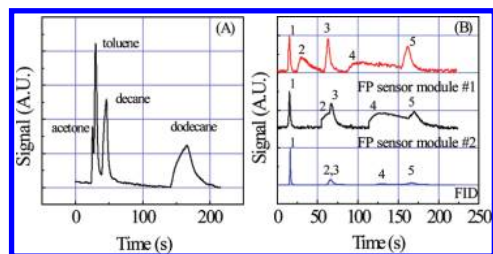


**Figure 7.** (A) Chromatograms of acetone, toluene, decane, and dodecane obtained from the PEG 1000 coated FP sensor module in the single-column system illustrated in Figure 1A. The retention time of each analyte was 25.4, 29.8, 46.0, and 165.8 s, respectively. (B) Chromatograms obtained from the two FP sensor modules in the tandem-column system illustrated in Figure 1B. The first FP sensor was coated with PDMS and the second with PEG 1000. For a comparison, an FID chromatogram obtained at the terminal end of the tandem-column system is also presented. All the peaks are normalized to the first peak. Curves are vertically shifted for clarity. The retention times for each analyte obtained from module no. 1 (module no. 2 and FID) were 15.0 s (15.7 and 15.7 s) for octane, 29.4 s (64.8 and 66.3 s) for DMMP, 63.1 s (67.3 and 66.3 s) for decane, 98.5 s (125.0 and 126.0 s) for DEMP, and 162.1 s (169.5 and 167.5 s) for undecane: 1, octane; 2, DMMP; 3, decane; 4, DEMP; 5, undecane.

at the terminal end of the single-column system (Figure 7A). Nonpolar analytes (i.e., acetone, toluene, and decane) that interacted weakly with the polar Carbowax-coated GC column had sharp peaks and short retention times of within 50 s, whereas the highly polar DMMP eluted around 150 s with a relatively broad peak.

In the tandem-column system plotted in Figure 1B, two FP sensors coated with PDMS and PEG 1000 were, respectively, installed at the end of the first (RTX-1-coated) and second (Carbowax-coated) GC column. A mixture comprising both polar and nonpolar analytes was used to investigate the system separation capability and selectivity. Comparison between the two chromatograms from the two FP sensors (Figure 7B) shows no significant change in retention time for alkanes (octane, decane, and undecane), owing to the weak interaction between nonpolar alkanes and the polar Carbowax-coated second column. In contrast, the retention times of the polar DMMP and diethyl methylphosphonate (DEMP) were considerably increased by the second column, leading to the coelution of DMMP and decane. Despite the coelution at the second column, the first FP sensor was able to provide a chromatogram from the first column, in which all the analytes were well-resolved. For a comparison, the FID was placed at the terminal end of the tandem-column system

(in the absence of the two FP modules) to carry out detection under the same experimental conditions. As expected, the retention times from the FID were very similar to those from the second FP sensor. Note that DMMP and decane from the FID were completely overlapped. Separate experiments using individual analytes confirmed that the overlapped peak indeed contained coeluted DMMP and decane.

## CONCLUSION AND FUTURE WORK

We have developed and characterized the FP sensor module based on-column  $\mu$ GC detector that can carry out rapid detection and have subnanogram detection limits. The FP sensor module is easily adaptable to traditional GC columns, enabling multiple on-column detection points along the column. Each sensor module can be tailored for a certain class of analytes, thus improving the detection sensitivity. It should be mentioned that, although all the results so far were obtained under the isothermal condition, the FP sensor modules are able to handle temperature programming, since the typical temperature ramping rate is slow compared to analyte adsorption/desorption process, as shown in Figure S2 in the Supporting Information. Detailed study in this regard, however, is beyond the scope of this paper.

Future work will be focused on optimizing the performance of the FP sensor based  $\mu$ GC detector, which includes lowering the detection limit by adding a reference channel to cancel out the temperature fluctuation induced noise and other types of noise, improving the adaptability by drilling a hole in a smaller fused-silica capillary or directly in a GC column using ultrafast laser ablation, coating a thinner polymer layer to improve the response speed, and improving the separation capability by temperature ramping. In addition, an array of FP sensors coated with different polymers will be employed in the  $\mu$ GC system to further increase the detection specificity.

## ACKNOWLEDGMENT

We acknowledge the financial support from the NSF (Grant Nos. ECCS-0729903 and DMR-0705974).

## SUPPORTING INFORMATION AVAILABLE

Additional information as noted in text. This material is available free of charge via the Internet at <http://pubs.acs.org>.

Received for review December 24, 2009. Accepted April 21, 2010.

AC902956D